

SenseNet:Deep Learning based Wideband spectrum sensing and modulation classification network

Shivam Chandhok, Himani Joshi, A V Subramanyam and Sumit J. Darak

Abstract—Next generation networks are expected to operate in licensed, shared as well as unlicensed spectrum to support spectrum demands of a wide variety of services. Due to shortage of radio spectrum, the need for communication systems (like cognitive radio) that can sense wideband spectrum and locate desired spectrum resources in real time has increased. Automatic modulation classifier (AMC) is an important part of wideband spectrum sensing (WSS) as it enables identification of incumbent users transmitting in the adjacent vacant spectrum. Most of the proposed AMC work on Nyquist samples which need to be further processed before they can be fed to the classifier. Working with Nyquist sampled signal demands high rate ADC and results in high power consumption and high sensing time which is unacceptable for next generation communication systems. To overcome this drawback we propose to use sub-Nyquist sample based WSS and modulation classification. In this paper, we propose a novel architecture called SenseNet which combines the task of spectrum sensing and modulation classification into a single unified pipeline. The proposed method is endowed with the capability to perform blind WSS and modulation classification directly on raw sub-Nyquist samples which reduces complexity and sensing time since no prior estimation of sparsity is required. We extensively compare the performance of our proposed method on WSS as well as modulation classification tasks for a wide range of modulation schemes, input datasets, and channel conditions. A significant drawback of using sub-Nyquist samples is reduced performance compared to systems that employ Nyquist sampled signal. However, we show that for the proposed method, the classification accuracy approaches to Nyquist sampling based deep learning AMC with an increase in signal to noise ratio.

I. INTRODUCTION

Automatic modulation classification (AMC) is a digital signal processing technique that aims to blindly estimate the modulation scheme of information signals present in the spectrum. AMC has been discussed widely for military and cognitive radio (CR) applications. For military applications, it is used for electronic warfare, surveillance, signal jamming and target acquisition [1]. Whereas in the CR applications, it is required for rate adaptation [2] and licensed user characterization to avoid the emulation attacks [3]. Hence, apart from determining the vacant bands, these applications also require the determination of modulation schemes of busy bands over a wide-range of spectrum. Thus, there is a need to perform both wideband spectrum sensing (WSS) and AMC on the detected busy bands.

The processing of a wideband spectrum demands high-speed Nyquist rate analog-to-digital converters (ADCs) which are not only computationally expensive but also area and power hungry. Recently, sub-Nyquist sampling (SNS) methods are being explored to overcome the drawbacks of Nyquist

sampling based digitization. These SNS methods exploit the sparsity of a wideband spectrum to perform digitization via low-rate ADCs [4]–[6]. Hence, to perform WSS and AMC (WSS-AMC), we require SNS based WSS-AMC.

Significant work has been done in the literature to perform SNS based WSS [4]–[6], however, very little attention has been made to SNS based AMC [7]–[9]. Various AMC methods [27]–[32] such as likelihood ratio and Bayesian classifier, wavelet classifier, cyclostationary feature classifier [40]–[52] and machine learning classifiers such as support vector machine (SVM) [11], k-nearest neighbor (KNN) [1], random forest (RF) [10] and neural networks [14] have been discussed in literature. However, all these classifiers deal with Nyquist sampled signal and may not work well under sub-Nyquist scenario. [7]–[9] are the only work which performed SNS based AMC. But these SNS-AMCs consider random SNS over a single preprocessed narrowband signal (i.e. on the modulated symbols of a baseband signals) for the modulation classification. Furthermore, no work has been done to perform AMC on the sub-Nyquist sampled wideband signal and SNS based joint WSS-AMC.

To overcome the limitations of existing works, in this paper, we propose a novel architecture called SenseNet which combines the task of spectrum sensing and modulation classification into a single unified pipeline. This architecture allows to perform WSS-AMC directly on the sub-Nyquist samples of the wideband signal. Hence, unlike the existing methods [27]–[32], it does not require pre-processed signal narrowband signal as its input. Furthermore, to analyse and compare the performance of the proposed SenseNet architecture with previously proposed AMC methods, we extend the analysis of the proposed SNS based AMC on the pre-processed in-phase and quadrature-phase (IQ) and amplitude-phase (AP) samples of the modulated symbols.

We conduct extensive experiments to analyse the effect of input signal representation on the classification accuracy by testing our model on sub-Nyquist sampled wideband signal, IQ samples and amplitude-phase (AP) samples, separately, for wide range of signal to noise ratio (SNR). We also test our model predictions under various channel impairments. We show that the classification accuracy of the proposed SNS-AMC approaches to the Nyquist sampling based AMC (NS-AMC) with an increase in SNR.

The contribution of this paper is many fold -

- 1) The proposed SenseNet provides an end-to-end pipeline which takes in multiband sub-Nyquist sampled wideband signal as its input and outputs the band status (vacant/busy) and modulation scheme of busy bands. To achieve this, the SenseNet first performs WSS followed by the modulation classification.
- 2) The proposed architecture uses a CNN based model (CNN_{SS}) for WSS to simultaneously classify all bands as vacant/busy making it more efficient than iterative approaches like orthogonal matching pursuit (OMP).

This work is supported by the funding received from CSIR, India under SRF Scheme and DST, India under INSPIRE faculty fellowship.

Shivam Chandhok is with Computer Science Department, IIT-Hyderabad, India-502285 (e-mail: {chandhokshivam}@iith.ac.in), Himani Joshi, Sumit J Darak and A V Subramanyam are with Electronics and Communications Department, IIIT-Delhi, India-110020 (e-mail: {himanij, sumit, subramanyam}@iiitd.ac.in)

Unlike OMP, the proposed deep learning architecture does not require prior knowledge of the sparsity of wideband spectrum.

- 3) Since the SenseNet perform AMC directly on the recovered wideband signal, we formulate a modified cross-entropy loss function which, based on the occupancy status of bands classifies the modulation scheme of detected busy bands.
- 4) We avoid the use of fully connected layers in our CNN models of the SenseNet. This unlike [27], [28], [30], enables the SenseNet to consider different size inputs (i.e. length of the input signal and no. of bands) without making any changes in the architecture.

Rest of the paper is organized as follows. The literature review of the existing WSS and AMC techniques are discussed in Section 2. Section 3 describes the signal model. The proposed end-to-end pipeline for WSS-AMC is presented in Section 4. Section 5 discusses the application of the proposed DLMC on unprocessed raw wideband samples, followed by its extension on the pre-processed IQ and AP samples in Section 6. The datasets and the implementation details of WSS-AMC are discussed in Section 7. The simulation results are presented in Section 8 followed by the conclusions in Section 9.

II. LITERATURE REVIEW

In this section, we review WSS and AMC techniques that are studied extensively in the literature.

A. WSS Methods

The extensive use of wireless devices and scarcity of radio spectrum has lead to extensive research in the field of WSS [15]–[17]. The use of conventional method for the processing of such a wideband signal requires very high Nyquist rate ADCs which are power and computationally inefficient. By taking the advantage of the sparsity of radio spectrum, SNS techniques like multi-coset sampling (MCS) and modulated wideband converter (MWC) have been proposed for the digitization of wideband signal. These SNS techniques use multiple low rate ADCs such that the average sampling rate \ll Nyquist Rate of the wideband signal. In MCS, each low rate ADC digitizes the wideband signal a unique time-offset. In [4], Multi-coset sampling (MCS) is applied where each ADC uniformly samples the incoming wideband signal with a unique time offset with respect to the other ADCs. Outputs of all ADCs are combined and subsequently reconstructed in the digital domain. However, MCS has several limitations. First, it requires an accurate time offset in the order of the Nyquist period (around pico-seconds), which is very difficult to generate in the analog domain. Second, the analog bandwidth of the required ADCs is too high. To overcome these limitations, the modulated wideband converter (MWC) was proposed [5]. In MWC, a specific analog mixing function is used, followed by a low pass filter at the input of each ADC. This results in need for a low analog bandwidth ADCs which are easily available. Furthermore, the MWC has been successfully realized in hardware [21] making it a state-of-the-art SNS approach. However, these approaches and subsequent extensions are limited to contiguous SNS.

For digital reconstruction of signal, extensive research has been focused on compressive sensing algorithms based on greedy approaches, l_1 norm minimization, and Bayesian methods for digital reconstruction in existing literature [62].

Although the greedy approaches offer less reconstruction accuracy when compared with l_1 norm minimization [63]–[65] based algorithm [65], their lower computational complexity makes them ideal for practical use. However, greedy approaches suffer from the drawback that they require prior knowledge of spectrum sparsity which might be unavailable in practice. The Bayesian approach tend to perform better than the above mentioned approaches as they offers better reconstruction accuracy than greedy algorithms [62] and lower computational complexity than l_1 norm minimization based algorithms.

After reconstruction, various algorithms can then be used to determine the status of frequency bands. These include matched filter [68], energy detection [69], Eigen-value based detectors and cyclostationary detector [70]. Interested readers may refer to [71] for more details about the advantages and drawbacks of these detectors.

In practice, the most commonly used techniques for WSS are greedy algorithms e.g thresholding algorithms [66], [67], [72], matching pursuit, OMP and its derivatives that build the solution iteratively [24]–[26]. These algorithms involve predicting the location of non-zero entries in the first step and then calculating the estimate of the sparse vector [19]. This process goes on at each iteration till the stopping criteria is reached. Several deep learning based approaches have also been proposed in the literature that integrate a deep/convolution neural networks or LSTM into this greedy iterative pipeline [19], [20], [22], [23]. However our proposed method is different from these approaches in several ways. Firstly, unlike OMP our algorithm does not require the knowledge of number of occupied bands beforehand. Secondly, the proposed method detects the vacant and occupied bands in a single forward pass through the CNN_{SS} network without the need for any iterative process. This makes our method more efficient than the above mentioned approaches at inference time and provides real time sensing of wideband signal. Also, through experimentation we show that the proposed method is better than OMP at detecting the status of bands (vacant/occupied).

B. AMC Methods

To determine the modulation scheme, various automatic modulation classification techniques such as likelihood ratio (LR) based classifiers, feature based (FB) classifier and intelligent learning (IL) classifiers have been discussed in the literature [12]–[14], [39]. LR based classifiers treat automatic modulation classification (AMC) as a multiple-composite hypothesis testing problem [39]. The modulation scheme is determined by applying the MLE (maximum likelihood estimation) criteria. The drawback with this approach is that the accuracy depends on the knowledge of channel and noise model, which varies dynamically in the real environment. To overcome this drawback of LR, FB classification methods [12], [13] are studied. FB classification uses variety of statistical features like moments, cumulants [12] and cyclostationary features [40]–[52] of the received signal for AMC. An extensive research has been focused on the analysis of these methods.

Recently, to further improve the accuracy of AMC, IL based AMC, which uses features and learning algorithm such as support vector machine (SVM) [11], k-nearest neighbor (KNN) [1], random forest (RF) [10] and shallow neural networks (NNs) [14] have become an active field of research. Out of these IL methods, NNs based AMC has shown the highest modulation classification accuracy [29]. NNs are deep learning

(DL) models and basically work as function approximators that recognize the underlying relation in data and extract complex patterns from it.

Most of the DL based AMC techniques use IQ samples as an input to the model. In [30], it is shown that a simple convolutional NN (CNN) model with just 2 convolution layers outperforms expert FB AMC methods by a considerable margin. Since then many researchers have tried to find the optimal deep learning architectures for AMC. In [27], [28] authors discuss the principle architectures used for the task of image recognition and adapt them to the task of AMC. An extensive study is conducted to analyse the effect of network depth, filter sizes and number of filters on the accuracy of classification.

The representation of input signal for IL algorithms is analysed in [29] and it has shown that the use of amplitude-phase samples with long-short term memory (LSTM) learning algorithm outperforms the IQ sample based CNN AMC [27], [28]. For further improving the performance at low SNR, [31], [32] use noise resistant features such as ambiguity function [31] and spectral correlation function [32] as an input feature to the deep learning models.

The existing AMC methods [27]–[32] work on narrow band Nyquist signal and thus can determine the modulation scheme of a single narrowband signal. These methods also require signal pre-processing (after the its detection via wideband spectrum sensing) before it can be fed to the classifier. But for WSS, we need to determine the modulation schemes of all detected narrowband signals present in the wideband signal. Hence, there is a need of a wideband-AMC and is the aim of the proposed AMC. To accomplish this task, we propose an end-to-end classification system that directly takes sub-Nyquist samples as an input, and then outputs the band status (i.e. vacant or busy) and modulation schemes of all detected busy bands.

III. SIGNAL MODEL

We consider a wideband signal consisting of multiple uncorrelated and disjoint narrowband signals of maximum possible bandwidth, B Hz. Mathematically, the received wideband signal, $x(t)$ can be modeled as

$$x(t) = \sum_{p=1}^P h_p(t) * a_p(t) e^{j2\pi f_p t} + \eta(t) \quad (1)$$

where P is the maximum possible number of transmissions in $x(t)$, $a_p(t)$ is the p^{th} modulated narrowband signal of carrier frequency f_p , $h_p(t)$ is the channel response faced by p^{th} signal, $\eta(t)$ is additive white Gaussian noise (AWGN) and $*$ is a convolution operator. The modulated narrowband signal, $a_p(t)$ can be represented as

$$a_p(t) = \sum_{l=1}^L g(t - lT_s) s_m(l) \quad (2)$$

where $g(t)$ is the impulse response of a root raised cosine (RRC) pulse shaping filter, T_s is the symbol period, s_m is the modulated symbol of M -order modulation scheme where $m \in \{1, 2, \dots, M\}$ and L is the length of symbol sequence. Similar to [4]–[6], we made the following assumptions on the wideband signal:

- 1) The wideband spectrum, $X(f)$, of maximum frequency, f_{max} is divided into N frequency bands of bandwidth, $B = \frac{f_{max}}{N}$.

- 2) The bandwidth of a narrowband signal $a_p(t)$ does not exceed B Hz.

For the ease of understanding, the frequently used notations are summarized in Table I.

TABLE I
NOTATIONS AND THEIR DEFINITIONS

Notation	Definitions
$x(t)$	Received wideband signal
P	Maximum number of active transmissions in $x(t)$
$a_p(t)$	p^{th} active transmission in $x(t)$
f_p	Carrier frequency of $a_p(t)$ active transmission
h_p	Channel response faced by p^{th}
$g(t)$	Impulse response of RRC filter
s_m	Modulated symbol
T_s	Symbol period
L	Number of symbols considered for Dataset 2 and 3
M	Order of a modulation scheme
N	Number of frequency bands in $x(t)$
$z[n]$	Sub-Nyquist samples
W	Number of sub-Nyquist samples considered for Dataset
K	Number of ADCs used for SNS ($K \ll N$)
β	Number of frequency bands considered for SNS
\mathbf{A}	Sensing Matrix of dimension $K \times \beta$
\mathbf{Z}	A $K \times W$ matrix of DTFT of $z[n]$
$\mathbf{X}(f)$	A $\beta \times W$ matrix containing FT of β frequency bands
$\tilde{\mathbf{X}}(f)$	Pseudo-reconstruction of $\mathbf{X}(f)$

IV. PROPOSED WSS-AMC

The proposed WSS-AMC consists of two phases: 1) Digitization and 2) Classification. The digitization phase digitizes the wideband signal, $x(t)$ via SNS based RF to digital conversion followed by the deep learning based model for WSS-AMC. The classification phase utilizes the digitized sub-Nyquist samples to identify the occupancy status followed by signal recovery and the determination of modulation scheme of all detected busy bands frequency bands present in the digitized signal.

A. SNS Architecture for Digitization

With the help of low rate ADCs, the SNS architecture aims to digitize a sparse wideband signal. As discussed in the Section II, various SNS architectures like MCS, RD, and MWC which sense the entire contiguous wideband spectrum and FRI based SNS method are available for the sub-Nyquist rate digitization. The discrete time Fourier transform (DTFT) of sub-Nyquist samples, $z[n]$, obtained from all these SNS models can be represented as

$$\mathbf{Z} = \mathbf{A}\mathbf{X}(f) \quad \forall f \in [0, B] \quad (3)$$

where \mathbf{A} is a $K \times \beta$ sensing matrix corresponding to the used SNS architecture, $\mathbf{X}(f)$ is a $\beta \times 1$ vector containing Fourier transform of β frequency sub-bands and β is the number of sensed frequency bands which in case of contiguous sensing is same as the total number of bands, N in $x(t)$ and for non-contiguous sensing it is the number of selected frequency bands.

B. Proposed End-to-End Pipeline of WSS-AMC

The block diagram of the proposed end-to-end pipeline for the WSS-AMC is shown in Fig. 1. The sub-Nyquist samples, \mathbf{Z} of a wideband signal and its corresponding sensing matrix \mathbf{A} are the inputs to the proposed pipeline (line1 Algorithm-1). The outputs of the end-to-end pipeline are status of each frequency band (i.e. vacant/busy) and the modulation scheme of detected busy frequency-bands. The proposed pipeline performs three tasks: 1) WSS with the help of a convolution neural network (referred to as CNN_{SS}), 2) Wideband signal recovery/reconstruction and 3) AMC on the reconstructed wideband signal. Unlike the existing classification models [27], [28], [30], we design our entire pipeline in such a way that it can handle different sized inputs, i.e different size of input signals, without making any changes to the architecture.

The input to the proposed WSS-AMC is the normalized pseudo reconstructed signal where the pseudo reconstructed signal(line2 Algorithm-1) $\tilde{\mathbf{X}}$ is computed as

$$\tilde{\mathbf{X}} = \mathbf{A}^\dagger \mathbf{Z} \quad (4)$$

The $\tilde{\mathbf{X}}$ is a complex valued signal of dimension $\beta \times Q$ where Q is the number of snapshots. Next, it is converted into a real matrix (line3 Algorithm-1) of size $\beta \times Q \times 2$ where its third dimension of size 2 represents the real and imaginary values of $\tilde{\mathbf{X}}$ (line4 Algorithm-1). Finally, for the faster convergence of CNN-SS training, the higher dimensional pseudo-reconstructed matrix is normalized in the range of (0, 1) (line5 Algorithm-1). Let us represent the normalized matrix as $\tilde{\mathbf{X}}_{norm}$ and is fed into the intelligent learning block as shown in Fig. 1. This block consists of two sub-blocks:

1) *Deep Learning based spectrum sensing (DLSS)*: The DLSS sub-block aims to determine the vacancy/busy status of frequency bands of the digitized frequency bands. To perform spectrum sensing, as shown in Fig. 2, we employ deep learning based convolutional neural network (CNN) which works in two modes: 1) Offline training mode and 2) Online inference mode (i.e. testing mode). During the offline training mode (Subroutine-1), CNN is trained using the supervised learning framework with the Dataset, $D1 = \{(\tilde{\mathbf{X}}_{norm,1}, l_1), (\tilde{\mathbf{X}}_{norm,2}, l_2), \dots, (\tilde{\mathbf{X}}_{norm,S}, l_S)\}$ where S denotes the number of samples (or observations) over which training is performed, $\tilde{\mathbf{X}}_{norm,s} \in \mathbb{R}^{N \times W \times 2}$ is the s^{th} pre-processed $\tilde{\mathbf{X}}_{norm}$ and $l_s \in \{0, 1\}^{N \times 1}$ is the label of s^{th} observation indicating the vacant (i.e. $l_s \in 0$) or busy (i.e. $l_s \in 1$) status of all N frequency bands of $\tilde{\mathbf{X}}_{norm,s}$.

The training process involves the minimization of a loss function, which is a measure of inconsistency between the

Algorithm 1: The SenseNet Algorithm

```

1 input: Sensing matrix  $\mathbf{A}$ , sub-nyquist samples  $\mathbf{Z}$ 
2  $\hat{\mathbf{X}} \leftarrow \mathbf{A}^\dagger \mathbf{Z}$ 
3  $X_{real} \leftarrow \text{Real}(\hat{\mathbf{X}}), X_{img} \leftarrow \text{Imag}(\hat{\mathbf{X}})$ 
4  $\hat{\mathbf{X}} \leftarrow \text{Concatenate}(X_{real}, X_{img})$ 
5  $\hat{\mathbf{X}}_{norm} \leftarrow \text{Normalize}(\hat{\mathbf{X}})$ 
6  $\theta_{ss} \leftarrow \text{SpectrumSensing}(\hat{\mathbf{X}}_{norm})$ 
7  $\hat{l} \leftarrow CNN_{ss}(\hat{\mathbf{X}}_{norm})$ 
8  $\mathbf{A}_{new} \leftarrow \text{select columns of } \mathbf{A} \text{ corresp. to occupied bands}$ 
9  $\hat{\mathbf{X}} \leftarrow \mathbf{A}_{new} * \mathbf{Z}$ 
10  $\theta_c \leftarrow \text{ModulationClassification}(\hat{\mathbf{X}}, \text{label})$ 
11  $\hat{k} \leftarrow \text{Classifier}(\hat{\mathbf{X}}_{norm}, \theta_c)$ 

```

Algorithm 2: Subroutine 1: Spectrum Sensing

```

1 Offline training mode
2 input: training set  $\chi = \{(\hat{\mathbf{X}}_{norm,i}, l_i)\}$  initialize CNN-SS
   weights  $\theta_{ss}$  randomly, learning rate  $\eta(t)$ ,  $t \leftarrow 0$ 
3 while not converge do
4    $t \leftarrow t + 1$ 
5   sample batch of datapoints  $(\hat{\mathbf{X}}_{norm,i}, l_i)$ 
6    $\hat{l} \leftarrow CNN_{ss}(\hat{\mathbf{X}}_{norm,i}, \theta_{ss})$ 
7    $L_{BCE}(\hat{l}, l) = -\sum_{i=1}^N (l[i] \log \hat{l}[i] + (1 - l[i]) \log(1 - \hat{l}[i]))$ 
8   update  $\theta_{ss} = \theta_{ss} - \eta(t) \nabla_{\theta_{ss}} L_{BCE}$ 
9 end
10 Output-  $\theta_{ss}$ 

```

Algorithm 3: Subroutine 2: Modulation Classification

```

1 Offline training mode
2 input: training set  $\chi = \{(\hat{\mathbf{X}}_{norm,i}, k_i)\}$  initialize Classifier
   weights  $\theta_c$  randomly, learning rate  $\eta(t)$ ,  $t \leftarrow 0$ 
3 while not converge do
4    $t \leftarrow t + 1$ 
5   sample batch of datapoints  $(\hat{\mathbf{X}}_{norm,i}, \text{label}_i)$ 
6    $\hat{l} \leftarrow \text{Classifier}(\hat{\mathbf{X}}_{norm,i}, \theta_c)$ 
7    $L_c = \sum_{k=1}^{n-bands} -y_k (\sum_i p_i \log(\hat{p}))$ 
8   update  $\theta_c = \theta_c - \eta(t) \nabla_{\theta_c} L_c$ 
9 end
10 Output-  $\theta_c$ 

```

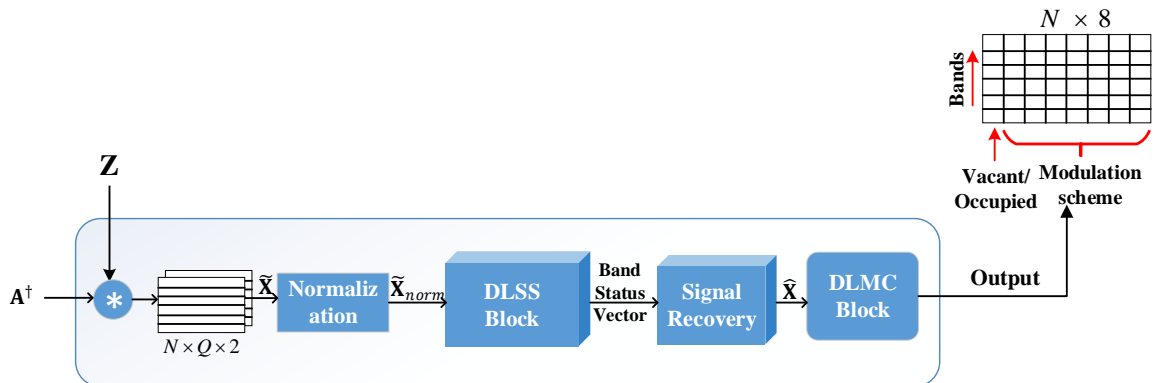


Fig. 1. Block diagram of the proposed End-to End pipeline of Wideband-AMC

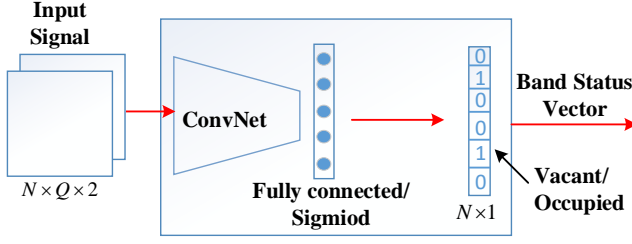


Fig. 2. CNN architecture for DL based spectrum sensing

predicted and actual label. Since more than one frequency band can be busy in a wideband spectrum, the problem can be classified as a multi-label binary classification. Hence, we use binary cross entropy as the loss function which can be calculated as

$$L_{BCE}(\hat{l}, l) = - \sum_{i=1}^N (l[i] \log \hat{l}[i] + (1 - l[i]) \log (1 - \hat{l}[i])) \quad (5)$$

where $l[i]$ and $\hat{l}[i]$ is the actual and predicted vacancy/busy status of i^{th} frequency band.

Furthermore, the network parameters are optimized using stochastic gradient descent algorithm, such that the training loss is minimized. The loss gradients are back propagated and used to update the learnable weights of the network at each iteration. This process is repeated till the validation loss no more decreases. The final output of training is the optimized parameters θ_{ss} (line 6 Algorithm-1).

After the training mode, the CNN model enters in the inference mode where it uses the trained weights of the model (i.e. θ_{ss}) to find the vacancy/busy status of real time wideband signal (line 7 Algorithm-1). The probability of detection of our proposed method and its comparison with other methods is done in section-8A.

Please note that to decide the architecture of deep learning model for spectrum sensing, we perform experiments with LSTM based as well as CNN based architectures. Through experiments it is validated that CNN perform much better than LSTM in deciding the band status (vacant/occupied) of the frequency bands.

We further perform experiment with different network depths and filter setting for the CNN based DL model. The filters used are of the form $1 \times n$ -taps where n -taps denotes the width of the convolution filter. We observe that filters with larger width perform better as compared to those with smaller width dimension and saturates when the width is increased further. The best classification accuracy is obtained using the architecture shown in Table II. Now, once we determine the vacancy/busy status of all N frequency bands, we perform signal recovery and then modulation classification on the busy frequency bands.

2) *Deep Learning based modulation classification (DLMC)*: The DLMC sub-block uses the estimated frequency bands status to determine the modulation scheme of the detected busy frequency bands. For AMC, we first perform the recovery of wideband signal (line 8-10 Algorithm-1) as shown in Fig. 3. Here, we take band status vector (determined by the CNN_{ss} and sensing matrix \mathbf{A} as input. Firstly, we generate a new sensing matrix \mathbf{A}_{new} by selecting the columns of \mathbf{A} which corresponds to the busy frequency bands followed by

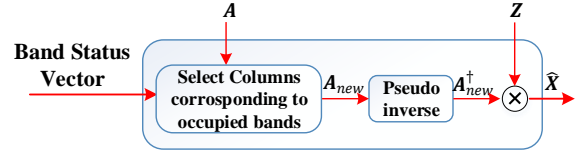


Fig. 3. Wideband Signal Recovery from the band status vector

the reconstruction of wideband signal. Mathematically, the recovery step can be written as

$$\hat{\mathbf{X}} = \begin{cases} \mathbf{A}_{new}^{\dagger} \mathbf{Z} & \text{if } \hat{l}_i = 1, \\ 0 & \text{if } \hat{l}_i = 0 \end{cases} \quad (6)$$

where $\hat{\mathbf{X}}$ is the recovered wideband signal, $\mathbf{A}_{new}^{\dagger}$ is the pseudo-inverse of new sensing matrix and \mathbf{Z} is the DTFT of sub-Nyquist samples. Next, to determine the modulation schemes of busy frequency bands, we directly pass the recovered wideband signal for the deep learning based modulation classification (Subroutine-2). This also consists of an offline training step which outputs the optimized parameters θ_c (line 1 Algorithm-1). These parameters are then used in the deep learning based modulation classifier to get the final classification output (line 12 Algorithm-1).

V. DLMC ON RAW WIDEBAND SIGNAL

Since unlike the existing AMCs, the proposed method does not require any pre-processing like intermediate frequency (IF) conversion and root raised cosine filtering on the busy frequency bands of $\hat{\mathbf{X}}$, we refer samples of reconstructed wideband signal as raw samples. Here, we explore convolutional neural network (CNN) and recurrent neural network (RNN) architectures for the modulation classification.

CNNs [34] can effectively model the spatial dependencies and extract robust features relative to a given classification task. They also involve sharing of parameters across various regions of the input, which makes them computationally more efficient than dense neural nets. On the other hand, RNNs make use of sequential information and capture temporal dependencies in data. Long short-term memory units (LSTM) [53], [54] are the most widely used variant of recurrent networks. Unlike conventional RNN models, they maintain an internal memory vector in addition to the hidden state vector at every time step. This helps them to remember the information from previous and current time steps more effectively. Thus, LSTM are better at modeling long-term dependencies in data which helps them to make better predictions.

Similar to the CNN modeling for spectrum sensing, discussed in the previous sub-section, to optimise the training weights for the CNN and LSTM models, we use stochastic gradient descent algorithm, such that the training loss

TABLE II
CNN ARCHITECTURE FOR SPECTRUM SENSING IN DLSS SUB-BLOCK

Layers	Filter Size	Number of Filters	Output Dimension
Input	—	—	14x299x2
Conv/relu	1x150	256	14x150x256
Conv/relu	1x100	128	14x51x256
Conv/relu	1x51	64	14x1x64
FC/sigmoid	—	—	14

(discussed in detail in section-7D) can be minimised. To finalize the architectures of both RNN and CNN based models, we perform extensive ablation study by varying their hyper-parameters discussed in section-8 in detail. For the RNN based model, we transform the 2 layered LSTM architecture in [29] and adapt it for our multiband-AMC task with some minor changes to boost accuracy. The LSTM network consists of N parallel (one for each band) neural network based modulation scheme prediction modules with shared weight. We perform the ablation study for different network depth and the size of hidden state vector in Fig. 10. The best performing architecture is shown in Fig. 5.

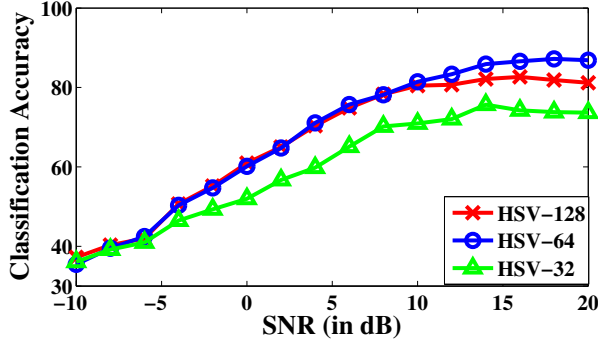


Fig. 4. LSTM Ablation Study on Raw Samples

While analysing the architecture of CNN for the AMC, we observe that the CNN architecture that best performs on raw samples is similar to the one used for the task of spectrum sensing. This is mainly due to the reason that the underlying signal used in both cases (i.e. for spectrum sensing and modulation classification) are similar. The CNN architecture for AMC is shown in Table III. The results of modulation classification on raw wideband signal and performance comparison of our methodology with other methods are discussed in section-8

TABLE III
CNN ARCHITECTURE FOR AMC ON RAW SAMPLES.

Layers	Filter Size	Number of Filters	Output Dimension
Input			$N \times Q \times 2$
Conv/ReLU	1×150	256	$N \times 150 \times 256$
Conv/ReLU	1×100	128	$N \times 51 \times 256$
Conv/ReLU	1×51	64	$N \times 1 \times 64$
Conv/ReLU	1×1	8	$N \times 1 \times 8$
Custom pool/softmax			$N \times 8$

VI. DLMC ON PRE-PROPOSED WIDEBAND SIGNAL

Since the existing AMC methods work on a single pre-processed (i.e. baseband and RRC filtered) Nyquist narrow-band signal, in this section we extend the proposed end-to-end pipeline of WSS-AMC to perform classification on the every pre-processed detected busy bands of the reconstructed sub-nyquist wideband signal. To perform AMC, three types of datasets of the pre-processed signals have been studied extensively in the literature. These datasets are: 1) IQ (in-phase and quadrature phase) samples, 2) Amplitude-Phase (AP) samples and 3) Constellation diagram images of modulation schemes. As real-time signal processing generates output in the form of samples, IQ and AP datasets are readily available

for AMC as compared to the constellation images. Hence, here, we explore IQ and AP samples of the pre-processed wideband signals. Furthermore, motivated by the fact that CNN based models perform well on IQ samples and LSTM based models perform well on AP samples [29], we analyse the CNN architecture on IQ samples and LSTM architecture on AP samples. In the next section we perform ablation study of CNN and LSTM architectures which are modified to take wideband signal as an input and simultaneously predict the modulation schemes of all detected busy bands.

A. CNN model Architecture

Since this is the first work that deals with modulation classification of multiband sub-nyquist signal, in this section we perform analysis to get the optimal CNN architecture for modulation classification on IQ samples of the multiband input signal. The architectures are designed in such a way that they give an $N \times 8$ output which includes the status of bands and the modulation schemes of busy bands (explained in detail in section 7D).

The baseline CNN architecture that we consider is shown in Table IV. It consists of three convolution layers, a custom average pool/softmax activation layer at the end. The last 1×1 convolution layer along with the custom pool layer aim to match the dimension of the output label and it is performed by averaging the input along the column dimension (i.e. L). Whereas the softmax activation layer associates the output with the probability of occurrence of every modulation scheme.

Since the input signal to our model can be viewed as a set of multiple one dimensional signal bands that have to be simultaneously classified according to their modulation scheme, we consider filter sizes of the form $1 \times n$ -taps as in [28]. The ablation study which helps us decide the baseline model's architecture is discussed in section 8.

Next, we discuss four state-of-the-art CNN architectures and use them to enhance the performance beyond our baseline performance

TABLE IV
BASELINE CNN ARCHITECTURE.

Layers	Filter Size	Number of Filters	Output Dimension
Input	-	-	$N \times L \times 2$
Conv/relu	1	64	$N \times L \times 64$
Conv/relu	1×3	64	$N \times L \times 64$
Conv	1×1	8	$N \times L \times 8$
Custom pool/softmax	-	-	$N \times 8$

1) *Network in Network (NiN)*: The Network in Networks architecture was introduced by et al in 2003 [35]. The architecture proposed the concept of micro networks that were integrated into the structure of a CNN to enhance the local modelling capability of the model. The authors argued that it was essential to compute abstract features for local patches before combining them into higher level concepts. The method can be viewed as an addition of 1×1 convolution layers. These 1×1 convolutions are similar to fully connected layers with tied weights acting independently at each pixel value to come up with a better abstraction on each local patch. The architecture of the NiN block and the model used is shown in Fig. 8 (a). The average pool custom layer instead of fully connected layers acts as a structural regularizer and helps us to train the network without any dropout at train time.

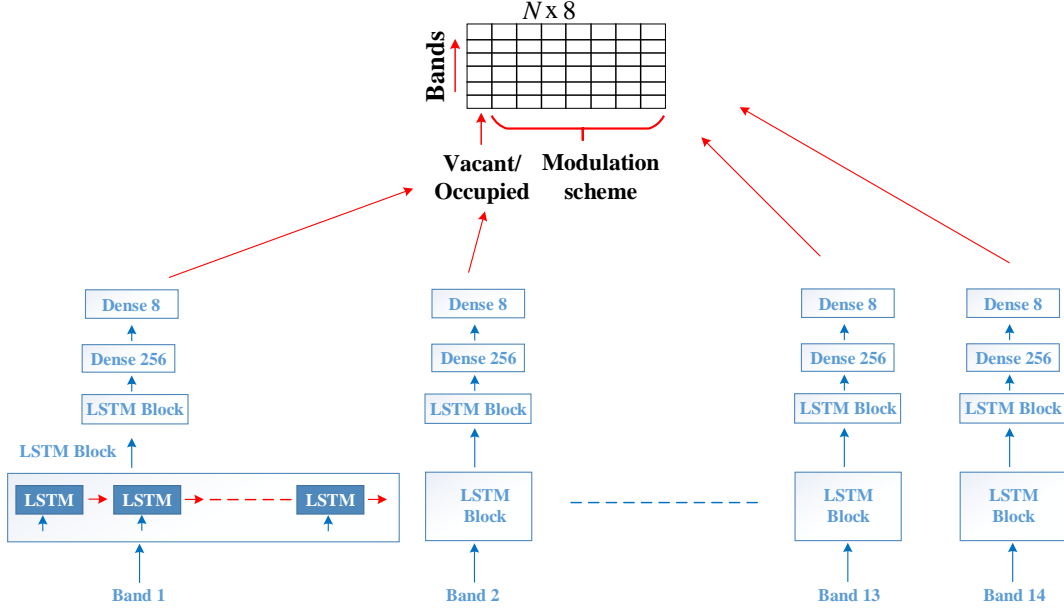


Fig. 5. LSTM architecture for Wideband-AMC

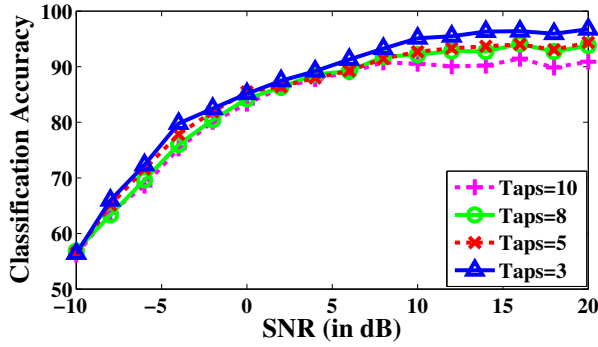


Fig. 6. Ablation study for baseline CNN on IQ samples for different values of n -taps

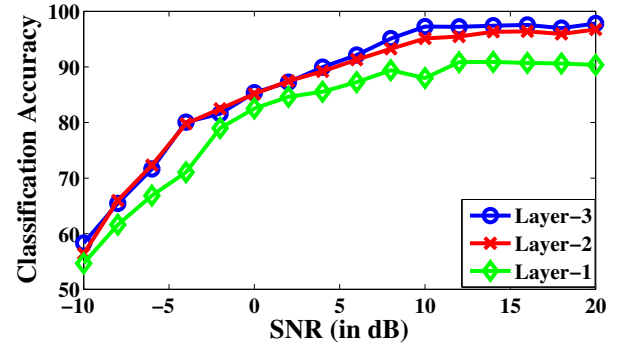


Fig. 7. Ablation study for baseline CNN on IQ samples for different numbers of layers

2) *Inception network*: The Inception architecture was introduced in [37]. The Inception block was based on the intuition of processing visual information at different scales before aggregating it so that the model can abstract features from different scales simultaneously. The block consists of three parallel paths each of which has different sized filters as shown in Fig. 8 (b). The information from various sized kernels is combined by concatenating it at the end.

3) *Residual network*: The Resnet architecture was introduced by He et al to mitigate the vanishing/exploding gradient problem faced while training deeper networks [36]. They addressed this issue by using skip connections between layers. The skip connections provide a direct path for the gradients to flow between layers without adding any extra parameters or increasing the model complexity. This stabilised the training process and prevented the degradation of accuracy as more layers were added. The architecture of the Residual block and

TABLE V
ARCHITECTURES FOR DIFFERENT VARIANTS OF BASELINE CNN MODEL

Nin		ResNET		Inception	
Layer	Output dimension	Layer	Output dimension	Layer	Output dimension
Input	$N \times L \times 2$	Input	$N \times L \times 2$	Input	$N \times L \times 2$
NiN Block	$N \times L \times 64$	ResNet Block	$N \times L \times 64$	Inception Block	$N \times L \times 192$
NiN Block	$N \times L \times 64$	ResNet Block	$N \times L \times 64$	Inception Block	$N \times L \times 192$
1×1 Conv/Relu	$N \times L \times 8$	1×1 Conv/Relu	$N \times L \times 8$	1×1 Conv/Relu	$N \times L \times 8$
Custom pool/softmax	$N \times 8$	Custom pool/softmax	$N \times 8$	Custom pool/softmax	$N \times 8$

the model used is shown in Fig. 8 (c).

4) *DenseNet architecture*: The Densenet architecture [38] uses concatenation instead of skip connections to combine feature maps. This leads to improved flow of information throughout the network. For each layer the feature maps of all preceding layers are used as inputs as shown Fig. 8 (d). The Densenet architecture mitigates the vanishing gradient problem which makes the training easier. It also encourages feature reuse and reduces the number of parameters which leads to model compactness and less overfitting encourages feature reuse.

Please refer Table V for the architecture details of NiN, Inception and Residual networks and Table VII for performance of these models at different SNR

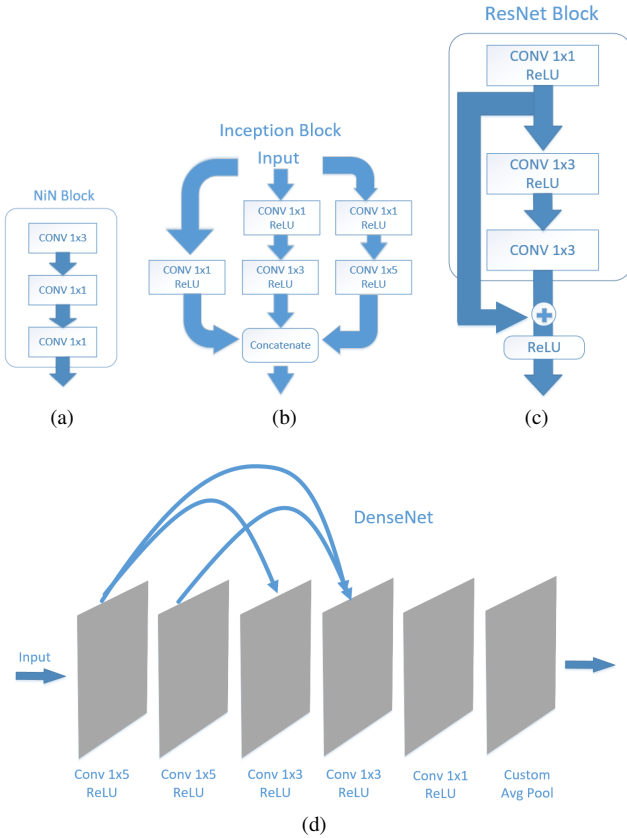


Fig. 8. Architectures for (a) NiN Block, (b) Inception Block, (c) Residual Block and (d) DenseNet network

B. LSTM Model

In [29] authors show that the representation of the input signal to the AMC network can lead to significant performance differences. The authors propose to use amplitude-phase samples as an input to a LSTM based model for the AMC of a pre-processed narrow band signal. Hence, we use an LSTM based network for AP wideband samples. The architecture of the network that we use is shown in IV-B2 (same as the one we used for raw samples)). Through extensive experiments we find that this architecture performs the best for the multiband AMC problem. We discuss the ablation for LSTM model in section 8

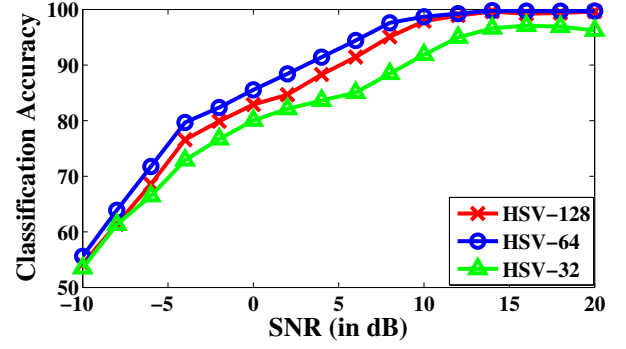


Fig. 9. Ablation study LSTM on AP pre-processed signal

VII. IMPLEMENTATION DETAILS

In this section, we discuss the dataset used for DLSS and DLMC task followed by the description of the proposed loss function used for DLMC on the pre-processed wideband signal. The dataset is generated synthetically using MATLAB tool. It consists of seven widely used modulation schemes namely: BPSK, QPSK, 16-QAM, 64-QAM, 128-QAM, 256-QAM and 8-PAM. The dataset is keyed by both modulation and SNR. We consider the SNR range from -10dB to 20dB at a step of 2dB.

A. Dataset for DLSS

To determine the vacancy/busy status of frequency bands of a wideband signal, we utilize the complex-valued normalized pseudo reconstructed signal, $\tilde{\mathbf{X}}_{norm}$ of size $N \times Q$. This signal is determined directly through the sub-Nyquist samples as discussed in Section IV-B. For generating the dataset, real and complex parts of $\tilde{\mathbf{X}}_{norm}$ are separated. Hence, the dataset is of the size $N \times Q \times 2$. Here, we considered $N = 14$ frequency bands and $Q = 299$ number of samples of each frequency bands. Since, this dataset is used to spectrum sensing, the label, l of each frequency band will either be vacant (i.e. $l = 0$) or busy (i.e. $l = 1$). Since this dataset allows spectrum sensing, we refer the dataset as **Dataset_{SS}**. We normalize this dataset in $\text{therange}(0,1)$ before passing it to the deep learning models.

B. Dataset for DLMC on Raw Wideband Samples

For determining the modulation schemes of the detected busy bands, we use the complex valued reconstructed wideband signal, $\tilde{\mathbf{X}}$ of size $N \times Q$. Similar to the **Dataset_{SS}**, this dataset is also separated into real and imaginary parts and hence, it is of size $N \times Q \times 2$. But since the dataset classifies the modulation schemes, its label, $l \in \{0, 7\}$ where $l = 0$ denotes the vacant frequency bands and $l \in \{1, 7\}$ belong to seven modulations schemes considered in the paper. Please note that from here on we refer this dataset for DLMC on raw wideband samples as **Dataset_{R-MC}**.

C. Dataset for DLMC on Pre-processed Wideband Samples

Like the existing AMC methods, the **Dataset_{P-MC}** consists of the pre-processed wideband samples. However, unlike , the pre-processing is done on the entire reconstructed wideband signal, $\tilde{\mathbf{X}}$. The labels of this dataset is same as that of the **Dataset_{R-MC}**. To perform DLMC on pre-processed wideband samples we considered the following two dataset:

Dataset_{P-MC1}: It considers the time domain IQ sample vectors

of pre-processed $\hat{\mathbf{X}}$. The dataset has a shape of $N \times L \times 2$ where $L = 256$ is the number of modulated symbols and the two vectors of third dimension denote in-phase and quadrature phase components of pre-processed $\hat{\mathbf{X}}$. We normalize this dataset in the range(0,1) before passing it to the deep learning models. The dataset is studied for three types of channel models:

Dataset_{P-MC} 1A - Dataset_{P-MC} 1 with AWGN channel.

Dataset_{P-MC} 1B - Dataset_{P-MC} 1 with flat fading and AWGN channel.

Dataset_{P-MC} 1C - Dataset_{P-MC} 1 with flat fading and AWGN channel with a doppler shift of 10 Hz.

Dataset_{P-MC} 2: It comprises of time domain amplitude-phase vectors (i.e. polar representation of IQ samples) of pre-processed $\hat{\mathbf{X}}$. Similar to **Dataset_{P-MC} 1**, it has a shape of $N \times L \times 2$ where the amplitude and phase part form two vectors of third dimension. The amplitude is $l-2$ normalized and phase (in radians) is normalized between the range -1 and 1 [29]. The dataset is also studied for for three types of channel models:

Dataset_{P-MC} 2A - Dataset_{P-MC} 2 with AWGN channel.

Dataset_{P-MC} 2B - Dataset_{P-MC} 2 with flat fading and AWGN channel.

Dataset_{P-MC} 1C - Dataset_{P-MC} 1 with flat fading and AWGN channel with a Doppler shift of 10 Hz.

D. Loss Function

Seven modulation schemes are considered for the classification, thus for each of the N bands, the output of the deep learning classifier (i.e. both CNN and LSTM) is a vector \hat{h} of unnormalized log probabilities and has the size of 1×7 . The values in vector \hat{h} are converted to probabilities by applying a softmax activation function which (for a particular band) is calculated as

$$\hat{p}_i = \text{softmax}(\hat{h})_i = \frac{\exp(\hat{h}_i)}{\sum_j \exp(\hat{h}_j)} \quad (7)$$

where \hat{p}_i is the predicted probability of $i^{th}(i=1,2,...,6,7)$ modulation scheme for a frequency band. This gives a output vector of size $N \times 7$

. The training loss for a particular frequency band depends on the status of the band. It is defined as the categorical cross entropy if the band is busy and zero if the band is vacant.

$$Loss_{per\ band} = \begin{cases} -\sum_i p_i \log(\hat{p}_i) & \text{if band is occupied,} \\ 0 & \text{if band is vacant} \end{cases} \quad (8)$$

where p_i is the actual probability distribution of the i^{th} modulation scheme for a particular frequency band. Next, the $N \times 7$ dimension output is concatenated with the band status vector from CNN-SS to give the final $N \times 8$ dimensional output \hat{k} . Thus, the entire loss function can be precisely expresses as

$$Loss = \sum_{k=1}^N -y_k (\sum_i p_i \log \hat{p}) \quad (9)$$

where y_k is the status (i.e. 0 for vacant and 1 for busy) of k^{th} frequency band.

E. Training Parameters and Tools

The neural networks are implemented using Keras [58] (with Tensorflow backend [59]) on Nvidia Cuda [60] enabled Quadro P4000 GPU. The weights of the models are initialized using default Keras initializers. We use an Adam optimizer whose parameters are set as learning rate = 0.001, $\beta_1 = 0.9$ and $\beta_2 = 0.999$ [61]. Furthermore, each dataset consists of 112,000 examples, out of which 75% (i.e 84,000 examples) are used for training and remaining (i.e 28,000 examples) are used for testing.

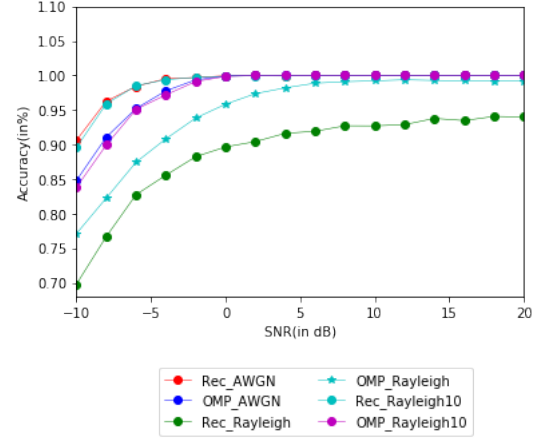


Fig. 10. Probability of detection for spectrum sensing

VIII. SIMULATION RESULTS

1) *Ablation Study for CNN:* We studied the classification performance to decide our baseline model architecture for different sizes of filter (i.e. n-taps), number of filter and depth of the network. Figure 6 shows the classification performance for various values of n-taps. We notice that smaller filter (n-taps = 3, 5) perform better than larger filters which is contrary to what we found in the case of raw sample inputs (as shown in Table III). Thus, we use small filter sizes (n-taps= 3, 5) in baseline CNN. Furthermore, the results obtained by varying the number of filters are very similar to the ones obtained in [28]. Thus, we use 64 number of filters for further analysis as it is efficient from both computation, memory and performance point of view. Also, as shown in Fig. 7, we observe no significant performance improvements when we increase the depth of our network beyond layer depth of 2. Hence, the baseline CNN uses 64 number of filter and network depth of 2.

2) *Ablation Study for LSTM:* To validate our LSTM based architecture, we carry out ablation study for hidden state vector size as shown in Fig. 9. It can be clearly seen that hidden state vector (HSV) size 32 underperforms especially at SNR ranges of 2-12 dB. We further notice that there is improve in performance as the HSV size is increased to 64. On further increasing the size to 128 we do not see any significant improvement in the average accuracy but the computational time increases. Thus we choose HSV=64 as the hidden state vector size for our model.

A. Results

In this section, we show the results of our proposed method on the task of spectrum sensing and modulation classification.

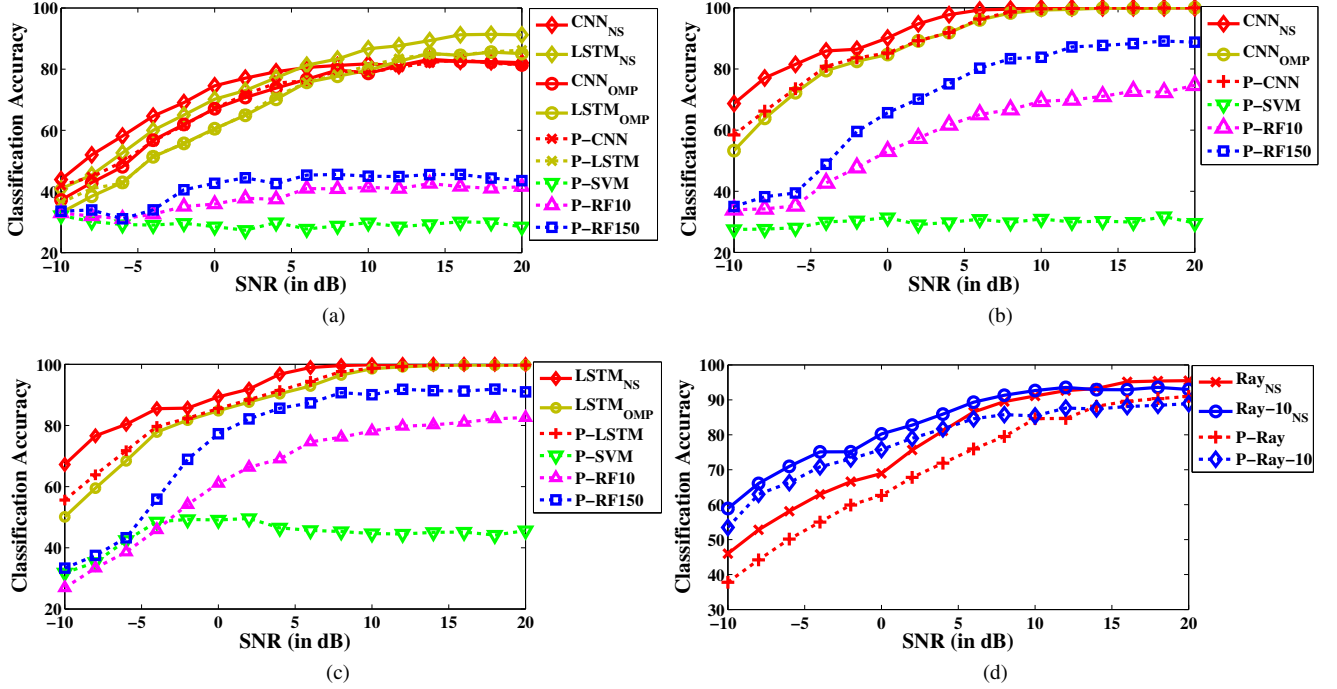


Fig. 11. Classification accuracy of the (a) proposed CNN-SS on **Datasetp-MC 2A** (b) proposed CNN-Inception on **Datasetp-MC 1A** (c) proposed LSTM on **Datasetp-MC 2B** (d) proposed LSTM on **Datasetp-MC 2C**

1) *Spectrum Sensing*: Fig 10. shows the results for probability of detection of occupied bands using our proposed method. For comparison, we choose the detection results of the OMP algorithm at different SNR. It can be seen clearly that at lower SNR values (till 5db) our method performs much better than OMP based detection. As the SNR increases further the performance of our method and OMP become similar and converge to the same value.

2) *Modulation Classification*: For modulation classification, we compare the performance of the proposed sub-Nyquist WSS-AMC on the raw wideband signal and the pre-processed IQ and AP samples of reconstructed wideband signal. We consider the performance of various machine learning (ML) algorithms to establish a baseline for our analysis. As the traditional ML algorithms cannot handle multiband signal as input, we pass only the detected busy bands one at a time sequentially for performance comparison. Furthermore, as the signal is sparse with very few busy bands, the classification accuracies are averaged over only the accuracy of busy bands for the fair comparison. The shown results have been generated for the MCS based digitization of sub-Nyquist sampling. However, similar observations are made with other SNS techniques. The performance comparison is done with the orthogonal matching pursuit (OMP) based AMC and other sub-Nyquist sampled machine learning AMCs. OMP based AMC uses OMP algorithm to perform WSS whereas the proposed method uses CNN deep learning model for WSS (as discussed in Section IV-B).

The classification accuracy comparison is performed for the raw wideband data, IQ samples and AP data samples under AWGN and Rayleigh Fading channel models. For all three data samples it is observed that the proposed WSS-AMC offers higher classification accuracy when compared to OMP based WSS-AMC and other ML based WSS-AMCs. The classification accuracy and comparison for different channel

models is discussed in detail below :

3) *AWGN channel condition*: The classification accuracy for raw wideband data, pre-processed IQ samples and AP samples under AWGN channel conditions at different SNR is shown in Fig. 11(a)-(c), respectively.

In Fig. 11(a)-(c) the subscript NS refers to the Nyquist sampled signal, OMP refers to signal reconstructed using OMP algorithm. The use of P-algorithm in the legends refers to sub-Nyquist signal sensed and recovered using proposed algorithm.

Fig. 11(a) shows the performance comparison for raw samples.

Here CNN refers to the proposed CNN_{SS} model and LSTM refers to the proposed LSTM architecture in fig5. For the raw samples, it is observed that, on averaging the classification accuracy over the entire range of SNRs, $CNN - SS$ offers 69.5% classification accuracy and is better than that for the LSTM model which achieves the average accuracy of 67.7%. For $CNN - SS$, it is observed that at high SNR (i.e 0db and above) the best case (i.e 0db) and worst case (i.e 20db) performance accuracies are (67.12) and (81.46) . The average accuracy on raw samples over SNR range 0-20db is 78 percent in the case of raw samples. Fig. 11(b) and (c) shows the performance comparison for IQ samples and AP samples.

Here CNN refers to the proposed CNN_{insep} model (given in table 5(c)) and LSTM refers to the proposed LSTM architecture in fig5. . It is observed that due to pre-processing on the reconstructed wideband signal, the classification accuracy of all classifiers is higher for the IQ samples and AP samples based AMC. For IQ samples the average accuracy for the proposed CNN based WSS-AMC is 88.95%. For high SNR it varies from 85.23 at 0db to 100 at 20db. Furthermore, The average accuracy over SNR range 0-20db is 96.42 percent for IQ samples. Whereas for the AP samples, the average classification accuracy achieved by the proposed LSTM based WSS-AMC is 88%. For high SNR it varies from 85.53 at 0db

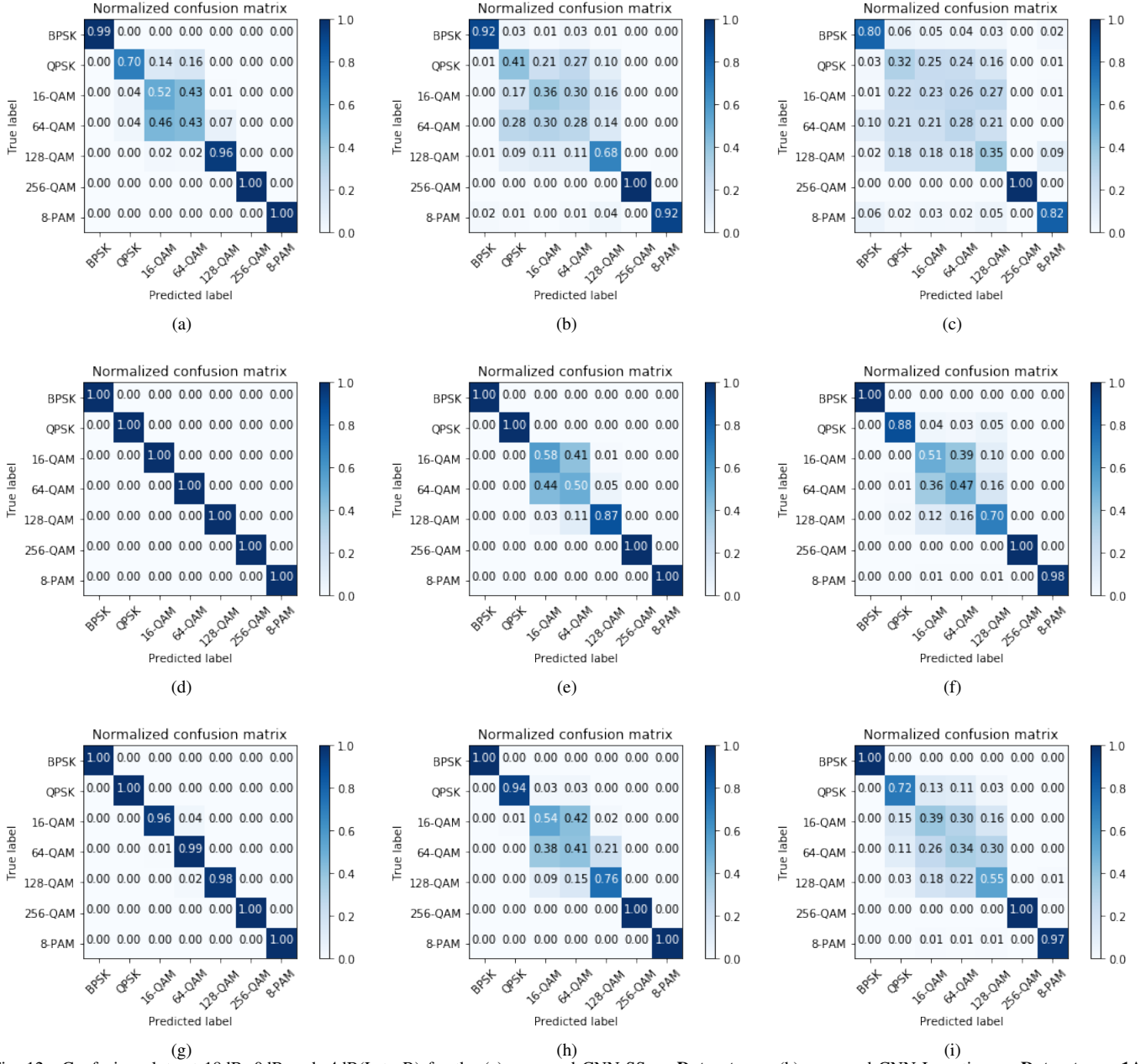


Fig. 12. Confusion plots at 18dB, 0dB and -4dB(L to R) for the (a) proposed CNN-SS on **Datasetr-MC** (b) proposed CNN-Inception on **Datasetp-MC 1A** (c) proposed LSTM on **Datasetp-MC 2A**

to 99.71 at 20db. Furthermore, The average accuracy over SNR range 0-20db is 95.83 percent for AP samples.

4) *Impaired channel condition:* Here, we consider the slow-fading and fast-fading with a Doppler shift of 10Hz for Rayleigh fading channel model. Under these channel models we find that the best performance is obtained using proposed LSTM based WSS-AMC on the AP samples. Fig. 11 (d) shows the classification accuracy of the proposed LSTM under Rayleigh Fading channel model. The average accuracy for Rayleigh fading channel conditions is 69.27 %. Under Rayleigh fading channel with a doppler shift, the average accuracy is found to be 76.48%. For all the scenarios, it is observed that the classification accuracy of the proposed SNS based WSS-AMC approaches to the NS based AMC with increase in SNR.

To understand the classifier performance and inter-class

discrepancies better, we analyse the confusion plots of the proposed WSS-AMC at -4db, 0db and 18db in Fig. 12. At 18db we can clearly see a sharp diagonal with almost perfect classification except for 16-QAM and 64-QAM. As the SNR reduces, the sharpness of the diagonal further reduces in the 16/64/256 QAM region. This happens due to the fact that the higher order classification like 16/64/256 QAM modulation schemes, the intersymbol distance decreases which makes it difficult for the classifier to distinguish out the correct QAM class.

IX. CONCLUSIONS

In this paper, we propose a deep learning based unified pipeline for real-time WSS and modulation classification of sparse wideband signal. The performance of the proposed SenseNet model is validated for different datasets and channel

TABLE VI
CLASSIFICATION PERFORMANCE COMPARISON OF SIGNAL RECOVERED USING PROPOSED
METHOD AND OMP RECONSTRUCTED SIGNAL

Method	Dataset _{R-MC}	Dataset _{P-MC 1A}	Dataset _{P-MC 2A}
OMP	68.9	88.11	86.64
Proposed	69.5	88.95	88

models. Simulation results show that the proposed model outperforms OMP in the task of spectrum sensing for all the different channel models considered. Being the first model to perform AMC on raw unprocessed wideband signal, we also show that the model gives 78 percent accuracy on raw wideband samples at high SNR(0-20dB) which is much higher than the performance of any other machine learning classifier. To validate our reconstruction method, we show that the modulation classification performance of our method is higher than that of OMP reconstructed signal. Furthermore, we also show the performance of the proposed model on IQ samples and AP samples. It is also shown that classification performance of the proposed SenseNet model approaches to that of Nyquist sampled AMC, with an increase in SNR for all datasets considered.

REFERENCES

- [1] M. W. Aslam, Z. Zhu, and A. K. Nandi, "Automatic modulation classification using combination of genetic programming and KNN," in *IEEE Trans. on Wireless Commun.*, vol. 11, no. 8, pp. 2742-2750, Aug. 2012.
- [2] M. Abu-Romoh, A. Aboutaleb, and Z. Rezk, "Automatic Modulation Classification Using Moments and Likelihood Maximization," in *IEEE Communications Letters*, vol. 22, no. 5, pp. 938-941, May 2018.
- [3] A. Alahmadi, M. Abdelhakim, J. Ren, and T. Li, "Defense against primary user emulation attacks in cognitive radio networks using advanced encryption standard," in *IEEE Trans. Inf. Forens. Security*, vol. 9, no. 5, pp. 772-781, May 2014.
- [4] R. Venkataramani and Y. Bresler, "Optimal Non-Uniform Sampling and Reconstruction for Multiband Signals," in *IEEE Transactions on Signal Processing*, vol. 49, no. 10, pp. 2301-2313, Oct. 2001.
- [5] M. Mishali and Y. C. Eldar, "From Theory to Practice: Sub-Nyquist Sampling of Sparse Wideband Analog Signals," in *IEEE Journal of Selected Topics in Signal Processing*, vol. 4, no. 2, pp. 375-391, April 2010.
- [6] H. Joshi, S. J. Darak, A. A. Kumar and R. Kumar, "Throughput Optimized Non-Contiguous Wideband Spectrum Sensing via Online Learning and Sub-Nyquist Sampling," in *IEEE Wireless Communications Letters*, vol. 8, no. 3, pp. 805-808, June 2019.
- [7] C. W. Lim and M. B. Wakin, "Automatic modulation recognition for spectrum sensing using nonuniform compressive samples," in *IEEE International Conference on Communications (ICC)*, Ottawa, ON, pp. 3505-3510, June 2012.
- [8] L. Zhou and H. Man, "Wavelet Cyclic Feature Based Automatic Modulation Recognition Using Nonuniform Compressive Samples," *78th IEEE Vehicular Technology Conference*, Las Vegas, Nevada, pp. 1-6, Sept. 2013.
- [9] S. Ramjee, S. Ju, D. Yang, X. Liu, A. El Gamal, Y. C. Eldar, "Fast deep learning for automatic modulation classification" in *arXiv:1901.05850*, Jan. 2019.
- [10] K. Triantafyllakis, M. Surligas, G. Vardakis, and S. Papadakis, "Phasma: An automatic modulation classification system based on Random Forest," in *IEEE Int. Symp. Dyn. Spectr. Access Netw. (DySPAN)*, Piscataway, NJ, USA, Mar. 2017, pp. 13.
- [11] J. Li, Q. Meng, Y. Sun, L. Qiu, and W. Ma, "Automatic modulation classification using support vector machines and error correcting output codes," in *Proc. ITNEC 2017*, pp. 60-63, Chengdu, China, Dec. 2017.
- [12] Gardner W.A. S "Signal interception: A unifying theoretical framework for feature detection," in *IEEE Trans. Commun.*, 1988;36:897906. doi: 10.1109/26.3769
- [13] Dandawate A.V., Giannakis G.B. "Statistical tests for presence of cyclostationarity," in *IEEE Trans. Signal Process.*, 1994;42:23552369. doi: 10.1109/78.317857.
- [14] Fehske A., Gaedert J., Reed J.H. "A new approach to signal classification using spectral correlation and neural networks," in *Proceedings of the First IEEE International Symposium on New Frontiers in Dynamic Spectrum Access Networks*, Baltimore, MD, USA. 811 November 2005; pp. 144150.
- [15] Kaabouch N., Hu W.C. "Handbook of Research on Software-Defined and Cognitive Radio Technologies for Dynamic Spectrum Management. Volume 2." in *IGI Global*, Hershey, PA, USA: 2014.
- [16] Al-Fuqaha A., Guizani M., Mohammadi M., Aledhari M., Ayyash M. "Internet of Things: A Survey on Enabling Technologies, Protocols, and Applications." in *IEEE Commun. Surv. Tutor.*, 2015;17:23472376. doi: 10.1109/COMST.2015.2444095.
- [17] Rawat P., Singh K.D., Bonnin J.M. "Cognitive radio for M2M and Internet of Things: A survey," in *Comput. Commun.*, 2016;94:129. doi: 10.1016/j.comcom.2016.07.012.
- [18] Arjouni Y, Kaabouch N. "A Comprehensive Survey on Spectrum Sensing in Cognitive Radio Networks: Recent Advances, New Challenges, and Future Research Directions," in *Sensors (Basel)*. 2019;19(1):126. Published 2019 Jan 2. doi:10.3390/s19010126
- [19] Palangi, Hamid, Rabab Ward, and Li Deng. "Convolutional deep stacking networks for distributed compressive sensing." in *Signal Processing* 131 (2017): 181-189.
- [20] H. Palangi, R. Ward, L. Deng, "Using deep stacking network to improve structured compressed sensing with multiple measurement vectors," in *IEEE International Conference on Acoustics, Speech and Signal Processing (ICASSP)*, 2013.
- [21] M. Mishali, Y. C. Eldar, O. Dounaevsky, and E. Shoshan, "Xampling: Analog to digital at sub-Nyquist rates," in *IET Circuits, Devices Syst.*, vol. 5, pp. 820, Jan. 2011.
- [22] A. Mousavi, A.B. Patel, R.G. Baraniuk, "A deep learning approach to structured signal recovery," in *arXiv:abs/1508.04065*.
- [23] H. Palangi, R. Ward, L. Deng, "Distributed compressive sensing: a deep learning approach," in *arXiv:abs/1508.04924*
- [24] Karahanoglu N.B., Erdogan H. "A orthogonal matching pursuit: Best-first search for compressed sensing signal recovery," in *Digit. Signal Process.* 2012;22:555568. doi: 10.1016/j.dsp.2012.03.003.
- [25] Donoho D.L., Tsaig Y., Drori I., Starck J.L. "Sparse Solution of Underdetermined Systems of Linear Equations by Stagewise Orthogonal Matching Pursuit," in *IEEE Trans. Inf. Theory*. 2012;58:10941121. doi: 10.1109/TIT.2011.2173241.
- [26] Tropp J.A., Gilbert A.C. "Signal Recovery from Random Measurements Via Orthogonal Matching Pursuit," in *IEEE Trans. Inf. Theory*. 2007;53:46554666. doi: 10.1109/TIT.2007.909108.
- [27] Timothy J. O'Shea, Tamoghna Roy, T. Charles Clancy "Over the Air Deep Learning Based Radio Signal Classification" in *IEEE Journal of Selected Topics in Signal Processing*, Volume: 12, Issue: 1, Feb. 2018
- [28] Nathan E. West and Timothy J. O'Shea "Deep Architectures for Modulation Recognition" in *2017 IEEE International Symposium on Dynamic Spectrum Access Networks (DySPAN)*
- [29] Sreeraj Rajendran, Wannes Meert, Domenico Giustiniano, Vincent Lenders, Sofie Pollin, "Deep Learning Models for Wireless Signal Classification With Distributed Low-Cost Spectrum Sensors", in *IEEE Transactions on Cognitive Communications and Networking*, vol. 4, no. 3, pp. 433-445, May 2018.
- [30] T.J. O'Shea, J. Corgan, T. C. Clancy, "Convolutional Radio Modulation Recognition Networks," in *Springer: Engineering Applications of Neural Networks (EANN)*, vol 629, pp. 213-226, Aug. 2016.
- [31] Ao Dai ; Haijian Zhang ; Hong Sun "Automatic modulation classification using stacked sparse auto-encoders" in *2016 IEEE 13th International Conference on Signal Processing (ICSP)*
- [32] Gihan J. Mendis ; Jin Wei ; Arjuna Madanayake "Deep learning-based automated modulation classification for cognitive radio" in *2016 IEEE International Conference on Communication Systems (ICCS)*
- [33] Timothy O'Shea ; Jakob Hoydis "An Introduction to Deep Learning for the Physical Layer" in *IEEE Transactions on Cognitive Communications and Networking*, Volume: 3, Issue: 4, Dec. 2017
- [34] A. Krizhevsky, I. Sutskever, and G. E. Hinton, "Imagenet classification with deep convolutional neural networks," in *Advances in neural information processing systems*, 2012, pp. 1097-1105, 2012.
- [35] M. Lin, Q. Chen and S. Yan, "Network in network," in *International Conference on Learning Representations*, 2014.
- [36] Kaiming He, Xiangyu Zhang, Shaoqing Ren, Jian Sun, "Deep Residual Learning for Image Recognition," in *2016 IEEE Conference on Computer Vision and Pattern Recognition (CVPR)*
- [37] Christian Szegedy ; Wei Liu ; Yangqing Jia ; Pierre Sermanet ; Scott Reed ; Dragomir Anguelov ; Dumitru Erhan, Vincent Vanhoucke, Andrew Rabinovich "Going deeper with convolutions," in *2015 IEEE Conference on Computer Vision and Pattern Recognition (CVPR)*
- [38] Gao Huang ; Zhuang Liu ; Laurens van der Maaten ; Kilian Q. Weinberger "Densely Connected Convolutional Networks," in *2017 IEEE Conference on Computer Vision and Pattern Recognition (CVPR)*
- [39] O.A. Dobre ; A. Abdi ; Y. Bar-Ness ; W. Su, "Survey of automatic modulation classification techniques: classical approaches and new trends," in *IET Communications* Volume: 1, Issue: 2, April 2007
- [40] Swami, A., and Sadler, B.M., "Hierarchical digital modulation classification using cumulants," in *IEEE Trans. Commun.*, 2000, 48, pp. 416429
- [41] Dai, W., Wang, Y., and Wang, J., "Joint power and modulation classification using second- and higher statistics," in *Proc. WCNC*, 2002, pp. 155158

TABLE VII
PERFORMANCE COMPARISON OF PROPOSED W-AMC ON DL CLASSIFIERS

Baseline Classifiers	AWGN					Rayleigh Fading					Rayleigh Fading with Doppler				
	-4 dB	2 dB	8 dB	14 dB	20 dB	-4 dB	2 dB	8 dB	14 dB	20 dB	-4 dB	2 dB	8 dB	14 dB	20 dB
Baseline	79.7	87.4	93.2	96.3	96.7	48.6	62.7	69.3	71.7	73.9	64.9	73.9	76.9	76.2	77.8
NiN	79.2	88.5	98.3	99.9	100	52.8	68.1	79.4	83.4	85.1	65.9	77	85.2	88.6	89.6
ResNet	79.9	88.6	98.2	99.9	100	52.5	66.6	79	83.3	86.6	66.6	76.9	84.6	89.1	90.8
Inception	80.4	88.9	98.2	99.7	100	53.7	67.7	79.5	85.4	88.9	67.5	77	85.5	90.3	91.2
Densenet	80	88.4	97.7	99.7	99.9	53.1	66.4	77.8	82.5	84.1	65.7	77.2	86	90	90.9

- [42] Hatzichristos, G., and Fargues, M.P., "A hierarchical approach to the classification of digital modulation types in multipath environments," in *ASILOMAR, 2001*, pp. 1494-1498.
- [43] Swami, A., Barbarossa, S., and Sadler, B. "Blind source separation and signal classification" in *Proc. ASILOMAR, 2000*, pp. 1187-1191.
- [44] Martret, C., and Boiteau, D.M. "Modulation classification by means of different order statistical moments," in *IEEE MILCOM, 1997*, pp. 1387-1391.
- [45] Marchand, P., Lacoume, J.L., and Le Martret, C. "Classification of linear modulations by a combination of different orders cyclic cumulants," in *Proc. ICASSP, 1998*, pp. 2157-2160.
- [46] Spooner, C.M. "Classification of cochannel communication signals using cyclic cumulants," in *Proc. ASILOMAR, 1995*, pp. 531-536.
- [47] Spooner, C.M., Brown, W.A., and Yeung, G.K. "Automatic radio-frequency environment analysis" in *Proc. ASILOMAR, 2000*, pp. 1181-1186.
- [48] Spooner, C.M.: "On the utility of sixth-order cyclic cumulants for RF signal classification" in *Proc. ASILOMAR, 2001*, pp. 890-897.
- [49] Dobre, O.A., Bar-Ness, Y., and Su, W. "Higher-order cyclic cumulants for high order modulation classification" in *Proc. IEEE MILCOM, 2003*, pp. 1121-117.
- [50] Dobre, O.A., Bar-Ness, Y., and Su, W.: "Selection combining for modulation recognition in fading channels." in *Proc. IEEE MILCOM, 2005*, pp. 2499-2505.
- [51] Dobre, O.A., Abdi, A., Bar-Ness, Y., Su, W. "Automatic radio-frequency environment analysis" in *Proc. ASILOMAR, 2000*, pp. 1181-1186.
- [52] Venalainen, J., Terho, L., and Koivunen, V. "Modulation classification in fading multipath channel," in *Proc. ASILOMAR, 2002*, pp. 1890-1894.
- [53] S. Hochreiter and J. Schmidhuber, "Long short-term memory," in *Neural Comput.*, vol. 9, no. 8, pp. 1735-1780, Nov. 1997.
- [54] A. Karpathy, J. Johnson, and L. Fei-Fei, "Visualizing and understanding recurrent networks," in *arXiv preprint arXiv:1506.02078*, 2015.
- [55] A. Karpathy, J. Johnson, and L. Fei-Fei, "Visualizing and understanding recurrent networks," in *arXiv preprint arXiv:1506.02078*, 2015.
- [56] N. Srivastava, G. E. Hinton, A. Krizhevsky, I. Sutskever, and R. Salakhutdinov, Dropout: A simple way to prevent neural networks from overfitting., *Journal of Machine Learning Research*, vol. 15, no. 1, pp. 1929-1958, 2014.
- [57] R. A. Dunne and N. A. Campbell, "On the Pairing of the Softmax Activation and Cross-Entropy Penalty Functions and the Derivation of the Softmax Activation Function," in *Proceedings of the Australian Conference on Neural Networks*, pp. 181-185, Melbourne, Australia, 1997.
- [58] F. Chollet, Keras, <https://github.com/fchollet/keras>, 2015.
- [59] M. Abadi, A. Agarwal, et al., "Tensorflow: large-scale machine learning on heterogeneous systems", 2015. Software available from tensorflow.org.
- [60] C. Nvidia, "Compute unified device architecture programming guide," 2007. <https://docs.nvidia.com/cuda/cuda-c-programming-guide/index.html>
- [61] D. P. Kingma and J. B., "Adam: A Method for Stochastic Optimization," in *International Conference on Learning Representations (ICLR)*, San Diego, California, May 2015.
- [62] Y. Arjoune, N. Kaabouch, H. E. Ghazi and A. Tamtaoui, "Compressive sensing: Performance comparison of sparse recovery algorithms," in *IEEE Computing and Communication Workshop and Conference*, pp. 1-7, USA, Jan. 2017.
- [63] R. Chartrand, "Exact Reconstruction of Sparse Signals via Non-convex Minimization," in *IEEE Signal Processing Letters*, vol. 14, no. 10, pp. 707-710, Oct. 2007.
- [64] E. J. Candes, M. B. Wakin, and S. P. Boyd, "Enhancing sparsity by reweighted l1 minimization," in *Journal of Fourier analysis and applications*, vol. 14, no. 5-6, pp. 877-905, Dec. 2008.
- [65] J. F. C. Mota, J. M. F. Xavier, P. M. Q. Aguiar and M. Puschel, "Distributed Basis Pursuit," in *IEEE Transactions on Signal Processing*, vol. 60, no. 4, pp. 1942-1956, April 2012.
- [66] J. D. Blanchard, M. Cermak, D. Hanle and Y. Jing, "Greedy Algorithms for Joint Sparse Recovery," in *IEEE Transactions on Signal Processing*, vol. 62, no. 7, pp. 1694-1704, April 2014.
- [67] T. T. Cai and L. Wang, "Orthogonal matching pursuit for sparse signal recovery with noise," in *IEEE Transactions on Information theory*, vol. 57, no. 7, pp. 4680-4688, July 2011.
- [68] S. Kapoor, S. Rao and G. Singh, "Opportunistic Spectrum Sensing by Employing Matched Filter in Cognitive Radio Network," International Conference on Communication Systems and Network Technologies, Jammu, India, 2011, pp. 580-583, July 2011.
- [69] M. Lopez-Benitez and F. Casadevall, "Improved energy detection spectrum sensing for cognitive radio," in *IET Communications*, vol. 6, no. 8, pp. 785-796, May 2012.
- [70] H.-S. Chen, W. Gao, and D. G. Daut, "Spectrum sensing using cyclostationary properties and application to IEEE 802.22 WRAN," in *Proc. of Global Telecommunications Conference*, pp. 3133-3138, Nov. 2007.
- [71] T. Yucek and H. Arslan, "A survey of spectrum sensing algorithms for cognitive radio applications," in *IEEE Communications Surveys & Tutorials*, vol. 11, no. 1, pp. 116-130, First Quarter 2009.
- [72] T. Blumensath and M. E. Davies, "Iterative hard thresholding for compressed sensing," in *Elsevier: Applied and computational harmonic analysis*, vol. 27, no. 3, pp. 265-274, Nov. 2009.